Sensors and Actuators B 243 (2017) 465–474

Contents lists available at ScienceDirect

Sensors and Actuators B: Chemical

journal homepage: www.elsevier.com/locate/snb

Pd-loaded SnO_2 ultrathin nanorod-assembled hollow microspheres with the significant improvement for toluene detection

Kan Zhang[a,*], Xin Yang[a], Yanzhe Wang[a], Yifei Bing[a], Liang Qiao[b], Zhongzhu Liang[c], Shansheng Yu[a], Yi Zeng[a,*], Weitao Zheng[a]

[a] College of Materials Science and Engineering, State Key Laboratory of Automotive Simulation and Control, Jilin University, Changchun 130012, PR China
[b] College of Science and Key Laboratory of Materials Design and Quantum Simulation, Changchun University, Changchun 130022, PR China
[c] State Key Laboratory of Applied Optics, Changchun Institute of Optics, Fine Mechanics and Physics, Chinese Academy of Sciences, Changchun 130033, PR China

ARTICLE INFO

Article history:
Received 4 May 2016
Received in revised form
25 September 2016
Accepted 28 November 2016
Available online 29 November 2016

Keywords:
SnO_2
Hollow nanostructures
Pd loading
Toluene
Gas sensor

ABSTRACT

Pd-loaded SnO_2 hollow microspheres have been successfully prepared via a facile one-pot hydrothermal route and subsequent Pd-loaded treatment without involving any templates, surfactants, or capping agents. The morphological and structural characterization confirms that Pd-loaded SnO_2 hollow microspheres are hierarchically constructed of numerous well-aligned rodlike SnO_2 subunits with ultrathin diameter of about 5–10 nm and monodisperse Pd particles with several nanometers in size. The time-dependent investigation demonstrates that the formation of hierarchical SnO_2 hollow spheres is driven by Ostwald-ripening mechanism. Furthermore, gas sensors based on pure and Pd-loaded SnO_2 have been fabricated. The Pd-loaded SnO_2 hollow microspheres exhibit relatively lower operating temperature, higher response and selectivity to toluene in comparison with that of pure SnO_2. Besides structural merits of ultrathin nanorod-assembled hollow and porous structure, the promotion of sensing performances can also be attributed to the contribution of catalytic Pd particles.

1. Introduction

Owing to a growing preoccupation with the deterioration of environments and air qualities in recent decades, there exists a tremendous demand for high-performance detecting and monitoring device. Gas sensors based on semiconducting oxides have brought forth a wide application prospect for various toxic, harmful, or explosive gases due to their straightforward principle, low cost, simple structure and easy manufacture [1,2]. The current tendency of semiconducting oxides in gas-sensing field is focused on the design and construction of oxides with various nanostructures on account of the fact that the structural merits of less-agglomerated configuration can guarantee a high specific surface area and surface accessibility [3]. In this regard, hollow architectures combined with sensitive functionality of permeable shells, especially the subunit-assembled hierarchical porous shells, perhaps possess obvious advantages for constructing high-performance sensors as these structures can provide accessible and high-activated shells for fast diffusion of gas molecules. To meet the requirements, several hollowing principles have been successfully developed to fabricate various hollow particles of diverse materials [3–7]. However, most available approaches are based on template-engaged routes, which often encounter disadvantages related to the increasing cost or complex operating steps, and the resulting hollow products are mostly built up from random aggregation of granular subunits but rarely from well-aligned rod-/sheetlike subunits. Rod-/sheetlike subunit-assembled hollow architectures represent a unique class of hollow structures characterized by their unique merits, such as primary building blocks with tunable shape, anisotropic texture correlated with exposed facets, and well-aligned porosity. There exists a fast growing interest on the engineering of hollow spheres with designable rod-/sheetlike subunits for further exploration of the widespread applications. Despite of considerable efforts being devoted to the preparation of these hollow structures, the exploration of a facile and economical one-pot route for the self-assembly of rod-/sheetlike subunits to form hollow particles remains challenging yet highly desirable.

Rutile SnO_2, as one of the most typical n-type semiconducting oxides for applications in gas sensors, has been generally applied for detecting different gases. Great efforts around the construction of novel nanostructures have successfully accomplished the intention on the improvement of sensing performances, because the sens-

* Corresponding authors.
E-mail addresses: zhangkan@jlu.edu.cn (K. Zhang), zengyi@jlu.edu.cn (Y. Zeng).

http://dx.doi.org/10.1016/j.snb.2016.11.153
0925-4005/

ing behaviors of oxides can be tuned via adjusting the intrinsical sensing reaction kinetics [8–14]. In this context, the establishment of SnO_2 hollow nanostructures has been widely acknowledged as a simple and effective approach to achieve high sensing performances [12–14]. Due to the special exposed facets and the possibility to achieve rod-/sheetlike subunits with fully depleted carriers, these hollow SnO_2 architectures supply a new opportunity for further improving the gas sensing performances. In addition, to meet the continuously improved demand for higher sensing characteristics, the decoration of noble metal or transition metal has been proved to be another effective strategy to dramatically ameliorate the sensing behaviors of SnO_2 via introducing intrinsically different reaction course [2]. For instance, Ramgir et al. have reported that the gas sensor based on Ru-doped SnO_2 nanowires shows better gas sensing performances to NO_2 compared with the pure homogeneity [15]. Kolmakov et al. have reported that the Pd-doped SnO_2 nanowires prepared by thermal evaporation method show distinctly enhanced H_2 sensing properties [16]. Lee et al. also found that Pd-doped SnO_2 nanorod thin films show distinctly enhanced H_2 sensing properties [17]. Korotcenkov et al. [18] reported that Pd doping SnO_2 thin films exhibit improved CO sensing performances. Vaishampayan et al. [19] found that the loaded Pd particles promote response of the sensors based on SnO_2 nanospheres towards liquid petroleum gas (LPG). The remarkable improvements in sensing behaviors based on the reported works about the doped SnO_2 nanostructures so far have put forward an exciting opportunity for further enhancing the performance of rod-/sheetlike subunit-assembled hollow nanostructures.

In this work, we report one-pot hydrothermal synthesis and subsequent Pd loading for Pd-loaded SnO_2 hollow microspheres, which are hierarchically constructed of numerous rodlike subunits with ultrathin diameter of 5–10 nm without the usage of any surfactant or capping agent. In particular, the crystallinity, structure, and morphology of pure and Pd-loaded SnO_2 hollow microspheres are elaborated. The formation process has been investigated through tracing the structural evolution with hydrothermal time, and a possible formation mechanism is discussed. Furthermore, the significant improvement of toluene sensing performances of Pd-loaded SnO_2 hollow microspheres can be anticipated on account of the ultrathin nanorod-assembled hollow structure and the catalytic effect of additional Pd particles.

2. Experimental procedures

2.1. Synthesis and characterization of pure and Pd-loaded SnO_2 hollow microspheres

All the chemicals are analytical grade and used without further purification. The typical synthetic procedure of the hierarchical SnO_2 hollow microspheres was as follows: 3 mmol of tin tetrachloride ($SnCl_4{\cdot}5H_2O$) was firstly dissolved in 30 ml distilling water at room temperature, then 18 mmol NaOH solution was slowly added into the above mixed solution under vigorous stirring. The uniform aqueous solution was transferred to a Teflon-lined stainless steel autoclave and heated to 180 °C for 2 h. The resultant precipitate was then centrifuged, washed by distilled water and absolute ethanol, and finally dried at 60 °C in the air for the collection of final product.

For Pd sensitization, ethanol solution of palladium chloride ($PdCl_2$) with a concentration of 2.5×10^{-3} mol/L was mixed with the as-prepared SnO_2 products (50 mg), where the weight ratio of Pd to SnO_2 is 2:100. The mixed solution was treated in an ultrasonic facility for 1 h to obtain a uniform solution, then the mixed precipitate was centrifuged, washed by absolute ethanol and dried at 60 °C for the collection of a gray precipitate, finally the mixture was annealed at 350 °C for 30 min in air atmosphere for collecting the Pd-doped SnO_2 microspheres.

The as-prepared products were characterized by powder X-ray diffraction (XRD, Rigaku D/max-2550) with Cu Kα radiation (λ = 0.15418 nm), field emission scanning electron microscope (FESEM, FEOL JSM-6700F, 8 kV), transmission electron microscope (TEM), selected-area electron diffraction (SAED), and high-resolution TEM (HRTEM, JEOL JEM-2100F, 200 kV), respectively. The surface area properties of sample were measured through measuring nitrogen adsorption-desorption isotherms with a Micrometrics ASAP2020 apparatus based on Brunauer-Emmett-Teller (BET) equation, and the pore size distribution was obtained by Barrett-Joyner-Halenda (BJH) method from the desorption branch of isotherms. X-ray photoelectron spectroscopy (XPS) measurement was carried out on a Scienta ESCA200 spectrometer equipped with a standard Al Kα excitation source.

2.2. Fabrication and measurement of gas sensing properties

The fabrication process of gas sensor based on our SnO_2 products can be described as follows: briefly, a certain amount of the final SnO_2 products were mixed with deionized water in a weight ratio of 4:1 to form a slurry, which then was pasted uniformly on ceramic tube with prefabricated gold electrodes to drying in air at room temperature. Then, a Ni–Cr alloy coil was placed inside the tube as a heater to control the operating temperature of the sensor devices. Finally, the sensor was constructed by connecting the corresponding junctions to the socket of the sensor. The schematic structure of the gas sensor is shown in Fig. S1 (Supplementary Materials) and the detailed fabrication process of gas sensor has been described elsewhere [20]. Sensing behavior measurements under the desired concentrations of testing gases were obtained via the static liquid gas distribution method in our previous report [21]. The response (R) of gas sensor is defined as the ratio (R_a/R_g) of the resistance of the sensor in dry air (R_a) to that in the testing gas (R_g). The response time (τ_{res}) and recovery time (τ_{recov}) are defined as the time taken by sensor to achieve 90% of the total response change in the case of adsorption and desorption, respectively.

3. Results and discussion

3.1. Structural and morphological characteristics

As shown in Fig. 1, XRD patterns reveal the phase purity and crystal structure of pure and Pd-loaded SnO_2 products. All the diffraction peaks in Fig. 1a can be well matched with the corresponding standard pattern of SnO_2 crystal with rutile structure in standard data file (JCPDS card No. 41-1445), although these discernable peaks possess broadening shape. No peaks from any other intermediates or crystalline phases are detected to confirm the high purity of the as-prepared SnO_2 products. As for Pd-loaded SnO_2 products, all the diffraction peaks can still be indexed to the standard rutile SnO_2 (Fig. 1b). Compared with the diffraction pattern of unloaded SnO_2 products, there exists a downward tendency for the peak intensity of Pd-loaded SnO_2. XRD analysis indicates that the loading of Pd particles decreases the crystallinity and structural integrity of SnO_2. Simultaneously, no obvious peaks corresponding to the loaded Pd or PdO*x* can be discernible, which may be ascribed to the fact that the Pd content is much lower in the Pd-doped SnO_2, compared to Sn or O.

The morphological and structural characteristics of the as-prepared unloaded SnO_2 products are illustrated by FESEM and TEM observations. From a panoramic FESEM image in Fig. 2a, it can be observed that the unloaded SnO_2 products are composed of numerous spherical aggregates, which exhibit rough surface with

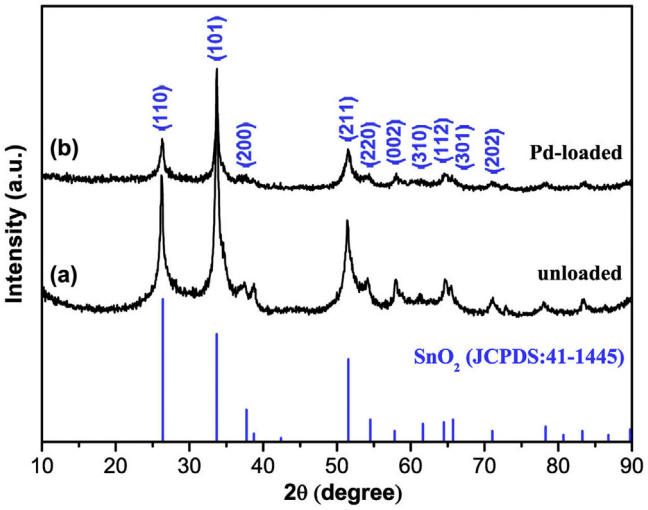

Fig. 1. The typical XRD patterns of the as-obtained (a) unloaded and (b) Pd-loaded SnO_2 products, respectively.

general size in the range of 500–800 nm. From the enlarged FESEM images in Fig. 2b, it can present the obvious superposition and aggregation of many similar homogenous rods from these SnO_2 microspheres, indicating that SnO_2 spheres exhibit a hierarchical structure with thin nanorods as the primary building blocks (inset of Fig. 2b). Further careful examination from some spheres with broken surface and their interior cavities, it confirms that the mentioned SnO_2 spheres are in fact hollow structures, as illustrated by arrows in Fig. 2b. The nanorod-assembled SnO_2 hollow spheres are further examined by TEM and HRTEM. The typical low-magnification TEM image in Fig. 2c shows that the size and shape of SnO_2 products are similar to the findings from the above FESEM observation. The shell of these hollow spheres is relatively uniform with a thickness of about 100 nm. Additionally, Fig. 2c and the corresponding ring-like SAED pattern further confirm that SnO_2 hollow spheres actually are polycrystalline texture and built up from many well-aligned rodlike subunits. HRTEM observation demonstrates that these SnO_2 rodlike subunits possess a small diameter of about 5–10 nm (Fig. 2d). The interplanar spacing of a single-crystalline SnO_2 nanorod is about 0.27 nm, corresponding to the (101) lattice planes of the tetragonal rutile crystal structure of SnO_2.

Furthermore, detailed structural analysis of Pd-loaded SnO_2 products has also been performed. As shown in Fig. 3a, the low-magnification TEM observation confirms that Pd-loaded SnO_2 products in fact exhibit the same spherical and hollow structure with uniform size. Further careful examination in Fig. 3a and b, a few dark spots can be observed on the tips of some rodlike subunits. The corresponding SAED pattern of Pd-loaded SnO_2 hollow spheres exhibits complex features, including polycrystalline diffraction rings of SnO_2 crystals and some ruleless diffraction spots, which may come from the PdO nanoparticles (inset of Fig. 3c). The typical high-magnification TEM image from one part of nanorod-assembled SnO_2 reveals that some additional nanoparticles with diameter of about 10 nm are well dispersed on SnO_2 nanorods, which are related to individual PdO particles and illustrated by dashed frames (Fig. 3b–c). The HRTEM image of the selected area in Fig. 3c exhibits two sets of well-resolved two-dimensional lattice fringes, which can be assigned to SnO_2 and PdO, respectively. As shown in Fig. 3d, the lattice spacing value from the rodlike object is about 0.274 nm, which is matched with the (101) planes of rutile SnO_2, and another marked spacing value of the particle is found to be 0.221 nm, corresponding to (110) planes of PdO. Notably, as for the Pd-loaded SnO_2 sample, the observations demonstrate that these monodisperse PdO nanoparticles have formed through randomly locating and growing during the Pd loading and subsequent anneal treatment. Thus, the less-agglomerated PdO particles on the SnO_2 nanorods may be very suitable for gas-sensing applications due to the high catalytic activity and large contact areas.

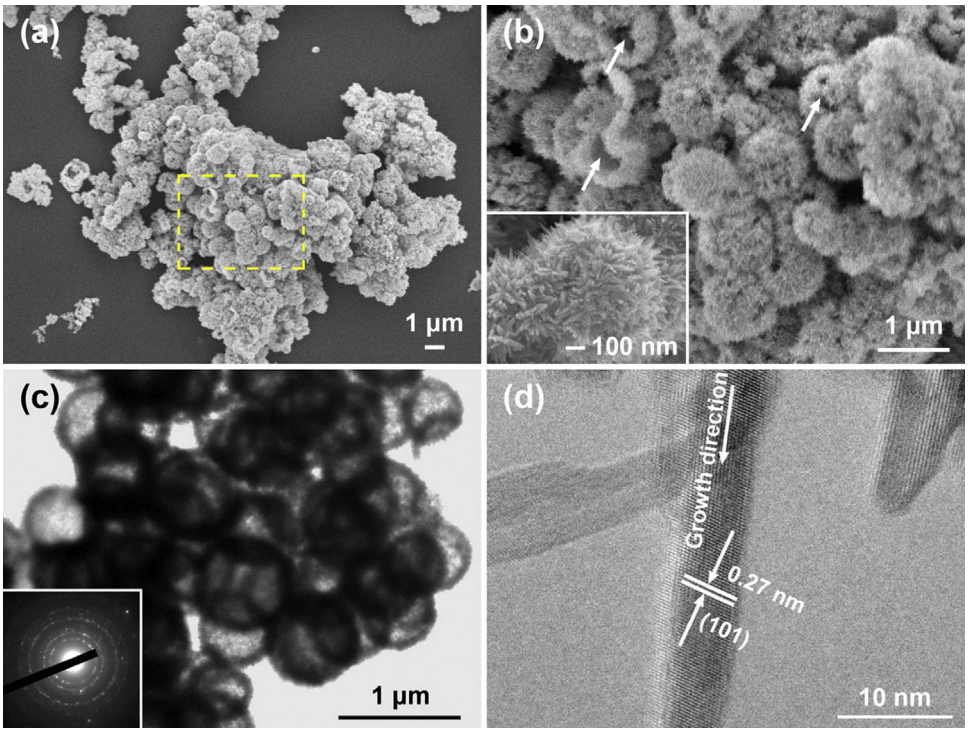

Fig. 2. (a) Low-magnification and (b) enlarged FESEM images, (c) TEM, and (d) HRTEM images of pure SnO_2 products. The insets of (b) and (c) show high-magnification FESEM image and SAED pattern of SnO_2 sample, respectively.

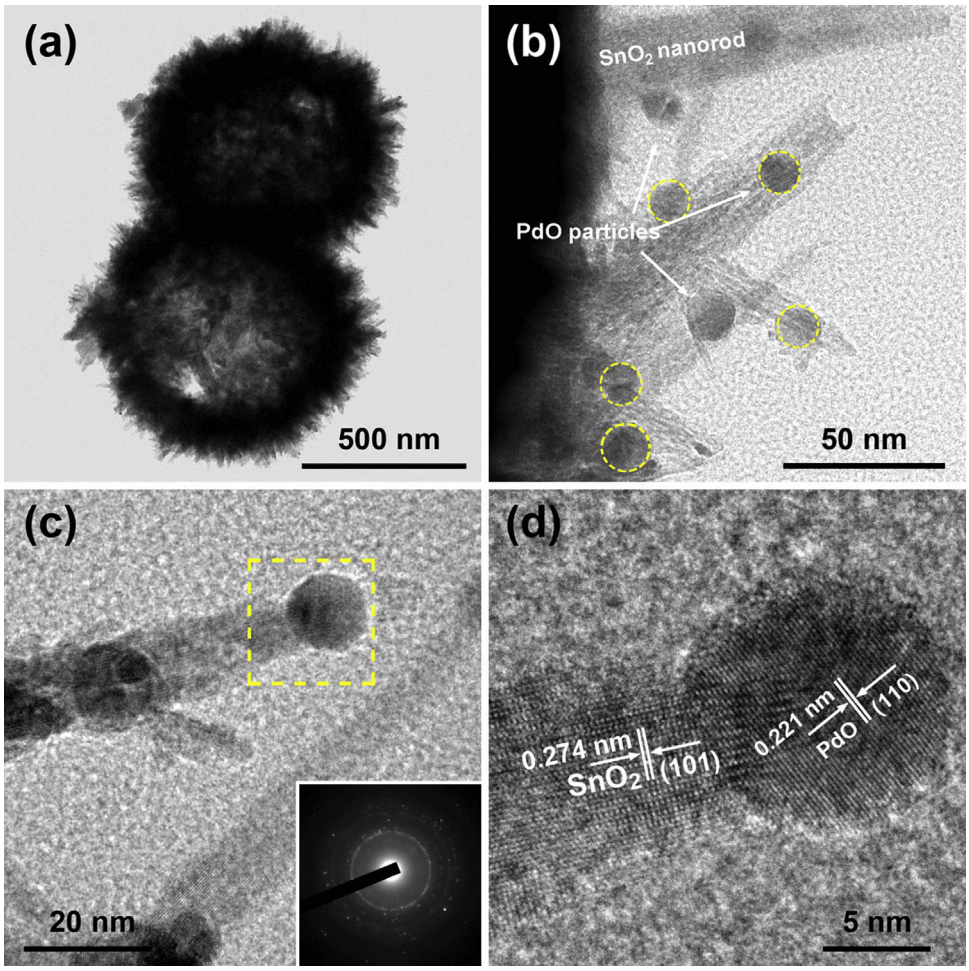

Fig. 3. (a,b) TEM images of Pd-loaded SnO_2 hollow microspheres and (c,d) HRTEM images of a typical Pd-loaded SnO_2 nanorod. The inset of (c) is a typical SAED pattern.

XPS analysis has also been performed to study the surface chemical composition and electronic states of the elements in the as-prepared Pd-loaded SnO_2. Clearly, the panoramic XPS spectrum shown in Fig. 4a reveals that two major sharp peaks in the range of 450–500 eV have binding energies of 495 eV and 486 eV. These peaks can be assigned to Sn $3d_{3/2}$ and $3d_{5/2}$, which are in good agreement with the values for the oxidation state of tin from SnO_2, respectively [22]. Among these sharp peaks, peak at binding energy of ~532 eV is in good accordance with O 1 s and the corresponding high-resolution spectra are shown in the upper inset of Fig. 4a. Obviously, it can be observed that the peak shows asymmetric shape, which can be separated to two major fitting peaks with binding energies of 531.9 eV and 530.5 eV, respectively. The peak at 531.9 eV can be characterized as surface-absorbed oxygen species (ie, O_2^- and O^-) and other peak at 530.5 eV could be regarded as typical surface lattice oxygen [23]. In addition, the high-resolution spectrum of Pd 3d is shown in the lower inset of Fig. 4a. The peaks with binding energies at 341.9 eV for Pd $3d_{3/2}$ and 336.8 eV for Pd $3d_{5/2}$ are in agreement with the values for PdO, respectively. Thus, XPS analysis confirms that a majority of Pd atoms in the as-prepared samples are present as PdO surface species [24], and probably small mole percent of PdO results in weak PdO peaks of XRD overlapping the SnO_2 peaks.

The BET specific surface area and pore size distribution of Pd-loaded SnO_2 hollow spheres are subsequently estimated through the nitrogen adsorption/desorption isotherms. As shown in Fig. 4b, there exists a typical type IV curve with a type H4 hysteresis loop from the nitrogen isotherms and the corresponding BET specific surface area is calculated to be 85.03 m^2g^{-1}. Using the BJH method and the desorption branch of the nitrogen isotherms, the calculated pore-size distribution indicates that the material contains an average pore size of 6.9 nm and a maximum at 1.9–2.2 nm, indicating the porous nature of Pd-loaded SnO_2 hollow nanostructures. Thus, the characteristic results demonstrate that the Pd-loaded SnO_2 hollow microspheres well inherit the local microenvironment including the interior cavities and penetrable high-activated shells for fast diffusion and transfer of gas molecules to reach or leave their surfaces.

According to the above-described experimental process, the formation of SnO_2 hollow microspheres in the present study does not involve any additional templates, surface modification or capping agents. It is obviously different from the general templating-engaged strategy, which always involves hard or soft templates with specific size in the first step and subsequently attracts metal complexes for their resulting nanoparticles near the hydrophilic shell of these templates [3]. To gain an insight into the formation mechanism of hierarchical SnO_2 hollow spheres, the hollowing evolution is traced with hydrothermal time. Fig. 5a–e show the time-dependent structural investigation before and after the hydrothermal treatment, and the results reveal that the final formation process can be separated into two distinct stages. Firstly, a large amount of metastable $Sn(OH)_4$ precursors are formed and aggregated at the initial moment as a result of the fast precipitation reaction with the presence of high feedstock concentration (Sn^{4+} and OH^-) [25]. It is energetically and structurally favorable that these aggregates subsequently undergo self-transformation to

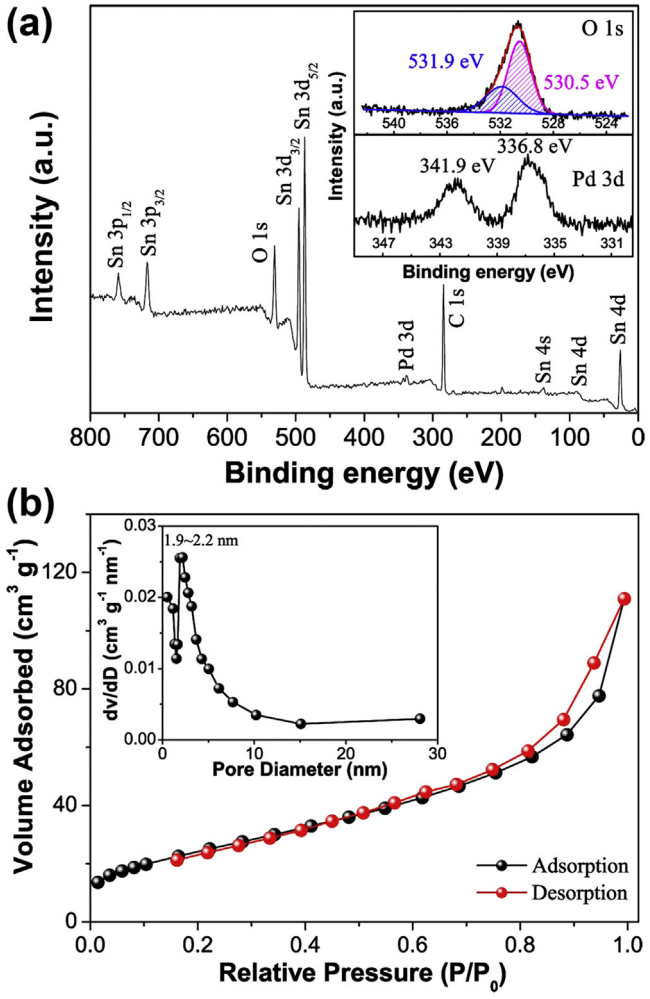

Fig. 4. (a) XPS spectra and (b) nitrogen adsorption and desorption isotherms of PdO-decorated SnO_2 hollow spheres. The upper and lower insets of Fig. 4a are the corresponding high-resolution O 1 s and Pd 3d spectra, respectively. The inset of Fig. 4b is the corresponding pore-size distribution calculated by BJH method from desorption branch.

form bigger but relatively more stable SnO_2 solid spheres by greatly reducing the interfacial energy of primary nanocrystals [26], as shown in Fig. 5a. As the hydrothermal reaction proceeds, the surface feature and hollow structure gradually change with the hydrothermal time from 10 min to 4 h, revealing that the dimension of hollow SnO_2 spheres is relevant to the reaction time (Fig. 5b–e). Specifically, during the early stage of hydrothermal process (10 min), some thin and small nanorods grow on the surface of the solid spheres, and there is no obvious clue that the small voids emerge inside the spheres (Fig. 5b). As the time is prolonged to 30 min, besides interior voids, outer nanorods can be observed with an increase in both the thickness and size (Fig. 5c). Simultaneously, the interior voids gradually become larger and eventually evolve to the well-defined spherical cavity after the reaction increasing to 1 h (Fig. 5d). When the hydrothermal process is allowed to proceed for a longer time of 4 h, the hollow structure still remains largely unaltered despite the severe aggregate of nanorods on the surface (Fig. 5e).

On the basis of the above mentioned investigation, the formation of nanorod-assembled hollow structure can be understood on account of the fact that the solid spherical interiors dissolve and redeposit to the outer surface. Firstly, solid spherical aggregates are formed at the initial stage due to the hydrolysis of tin precursors under hydrothermal conditions. With increasing hydrothermal time, the outer surface of solid aggregates begins to crystallize and form a thermodynamically stable thin shell of well-crystallized SnO_2, which is in equilibrium with respect to the hydrothermal surrounding and the corresponding reaction can be expressed in Eq. (1). However, unlike the outer crystalline shell, the interior of aggregates still remains out of equilibrium with the surrounding due to the rapid spontaneous nucleation and insufficient crystallization. Hence, the inner amorphous SnO_2 has a strong tendency to dissolve and outward diffuse, followed by recrystallization. The newly reproduced SnO_2 crystallites will preferentially deposit onto the crystalline outer shell, serving as the lattice-matched templates, to increase its thickness rather than to generally form additional self-aggregated particles, since the former seems to be a more effective way to reduce the total system energy [27].

$$Sn^{4+} + 4OH^- \leftrightarrow Sn(OH)_4 \leftrightarrow SnO_2 + 2H_2O \quad (1)$$

$$Sn(OH)_4 + 2OH^- \leftrightarrow [Sn(OH)_6]^{2-} \leftrightarrow SnO_2 + 2H_2O + 2OH^- \quad (2)$$

On the other hand, the anisotropic growth habit of recrystallized SnO_2 is restrained during the early stage of hydrothermal process because of the shortage of growth complexes $Sn(OH)_6^{2-}$ [28],

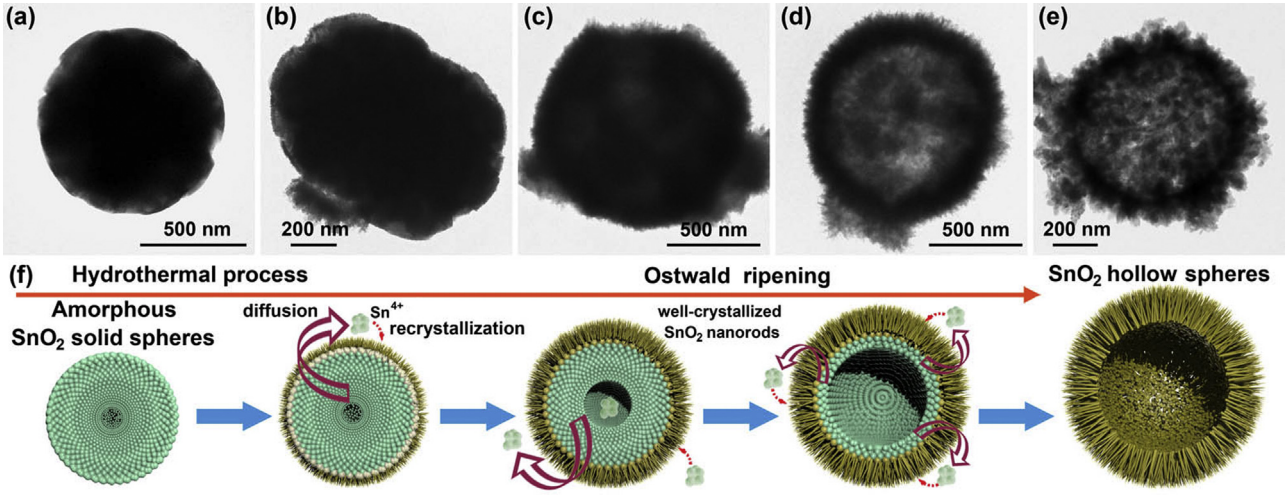

Fig. 5. The representative TEM images for hollowing evolution of SnO_2 samples prepared with different hydrothermal time: (a) 0 min, (b) 10 min, (c) 30 min, (d) 1 h, and (e) 4 h. (f) Schematic illustration of the possible formation process for nanorod-assembled SnO_2 hollow spheres.

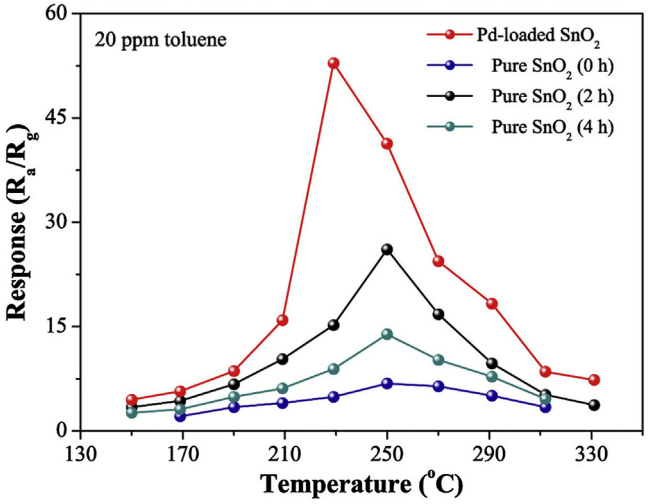

Fig. 6. Response versus operating temperature of sensors based on pure and Pd-loaded SnO_2 nanostructures to 20 ppm toluene, respectively.

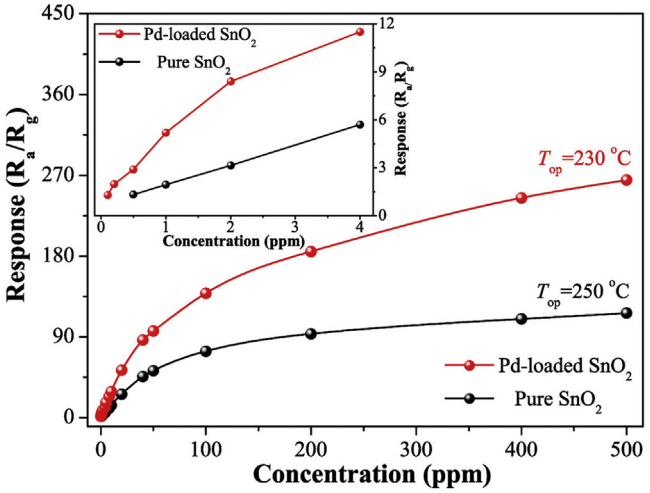

Fig. 7. Response curves of pure and Pd-loaded SnO_2 microspheres to various toluene concentrations, respectively. The inset shows a quasi-linear dependence of the response of different SnO_2 on toluene concentration within 0.1–4 ppm.

which can be attributed to the fast consumption of Sn^{4+} in the initial precipitation reaction. As the hydrothermal time increases, the unceasing outward diffusion of free Sn^{4+} not only recrystallizes to increase the thickness of crystalline shell, but also recombines with OH^- to form a large number of growth complexes $Sn(OH)_6^{2-}$, which promote the anisotropic growth of crystalline SnO_2 to form rodlike structure according to Eq. (2). Further prolonging the hydrothermal time, the continuous dissolution of core materials accelerates the radial growth of crystalline SnO_2, eventually leading to the formation of well-developed spherical cavity and nanorod-aggregated outer shell. This process is driven by the localized Ostwald-ripening or chemically induced self-transformation [4], as schematically illustrated in Fig. 5f.

3.2. Toluene sensing properties

Benefiting from the above-mentioned less agglomerated configuration, the Pd-loaded SnO_2 hollow spheres can guarantee a high-activated contacting surface and numerous diffusion channels for the efficient mass transfer of gas molecules to accomplish the fast adsorption and desorption. Thus, excellent gas-sensing performances of sensor based on our Pd-loaded SnO_2 nanostructures can be anticipated. For the comparison of gas sensing performances, sensors based on different SnO_2 products obtained with hydrothermal time of 0 h, 2 h, and 4 h are also fabricated, respectively, and the target gas is focused on the toxic and inflammable toluene (C_7H_8).

Due to the high dependence of gas sensing characteristics on operating temperature, the variation of responses to toluene with a typical concentration of 20 ppm has firstly been investigated to determine the optimal working temperature of our SnO_2 sensors. As shown in Fig. 6, it can be revealed that the sensors based on pure and Pd-loaded SnO_2 samples to toluene with the same concentration have similar sensing curves with parabolic shape, indicating that the response gradually increases with the improved operating temperature to reach its maximum and then decreases with further raising the temperature. This behavior can be ascribed to the subtle dynamic balance between the adsorption and desorption process of gas molecules under the control of the operating temperature. For the pure SnO_2 sensors, the obvious discrepancy of responses can be attributed to the organization of SnO_2 nanostructures depicted in Fig. 5, indicating that hollow structure with thin rodlike subunits is very beneficial for high response character. Specifically, the response of sensor based on pure SnO_2 hollow spheres (2 h) to 20 ppm toluene reaches its maximum of 26.1 at 250 °C. As for sensor based on Pd-loaded SnO_2, it exhibits higher responses during the whole testing temperature range and the significant improvement of the highest response is about 52.9 at a slightly lower operating temperature of 230 °C. The notable difference of responses between pure and Pd-loaded SnO_2 can be attributed to the catalytic activity of additional Pd. In view of maximizing performance, the optimal working temperature would be set at 230 °C and applied in all the sensing investigations hereinafter.

Response variation of sensors based on pure and Pd-loaded SnO_2 hollow microspheres along with toluene concentration is subsequently studied at their corresponding optimal operating temperature. As shown in Fig. 7, it demonstrates that responses of all sensors are sharply increasing with the increase of toluene concentration at relatively low range, then show a gradual slowdown of the increasing tendency, and finally are close to certain equilibrium, indicating that gas sensors become more or less saturated. Obviously, the response of Pd-loaded SnO_2 has a faster increasing tendency than that of unloaded SnO_2 until the concentration is increasing up to 400 ppm. There is an approximate linear relation between the response and toluene concentration within 40 ppm. As shown in the inset of Fig. 7, it exhibits the relationship between the responses of different sensors and toluene concentration with the concentration in the range of 0.1–4 ppm. The distinguishable lowest concentration of Pd-loaded SnO_2 sensor is 0.1 ppm with the response value of 1.29 while the lowest detecting concentration of pure SnO_2 is 0.5 ppm with the response value of 1.32. The results confirm that the limitation of pure SnO_2 hollow spheres for toluene detection can be further extended via the promotional effect of Pd nanoparticles.

Since selectivity for a target gas among different interfering gases, especially those having similar physicochemical properties, is an important aspect of sensing performance in the practical applications, the selective histogram of sensors based on pure and Pd-loaded SnO_2 has also been investigated to various kinds of gases. As shown in Fig. 8, it can be evident that sensor based on Pd-loaded SnO_2 exhibits relatively higher responses to all the testing gases than that of pure SnO_2 sensor at different operating temperatures. Specifically, Pd-loaded SnO_2 sensor exhibits the highest response value of 52.9–20 ppm toluene, which is over four times higher than the obtained response (12.3) to benzene and more times higher than that to other potential interfering volatile organic compounds (VOCs), such as acetone, ethanol, and methanol. The results confirm that Pd-loaded SnO_2 sensor displays a good selectivity to toluene at

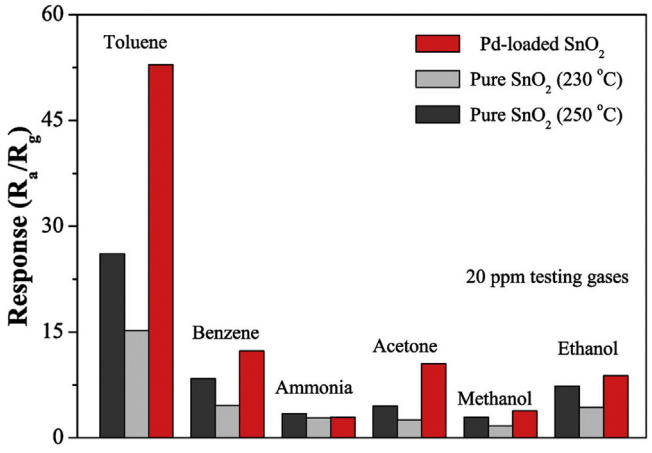

Fig. 8. Selectivity of sensors based on pure and Pd-loaded SnO_2 to 20 ppm various testing gases.

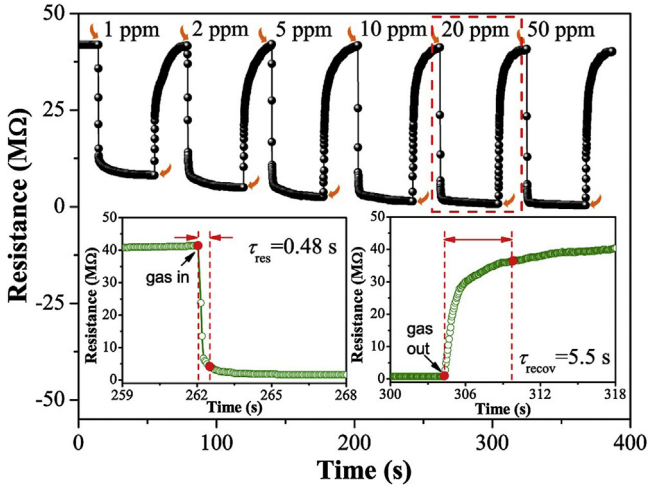

Fig. 9. Dynamic toluene sensing transients of Pd-loaded SnO_2 hollow spheres to toluene with the increasing concentration. The insets show the corresponding response time (τ_{res}) and recovery time (τ_{recov}) of Pd-loaded SnO_2 to 20 ppm toluene, respectively.

its optimal operating temperature of 230 °C. Meanwhile, compared with the response of Pd-loaded SnO_2 sensor to these gases, much lower responses but similar selective characters are obtained from pure SnO_2 sensor under the same testing process at different operating temperature of 230 °C and 250 °C. The improved selectivity of Pd-loaded SnO_2 compared to pure SnO_2 seems to be attributed to the catalytic discrepancy between the sensing materials and various gases.

The response and recovery time, as another important aspect of gas-sensing characteristics, has also been investigated. Fig. 9 presents six dynamic and continuous response periods of sensor based on Pd-loaded SnO_2 to toluene with the incremental concentration from 1 to 50 ppm. Apparently, the sensor exhibits the excellent response capability and recovery capability with respect to different toluene concentrations. As shown in insets of Fig. 9, the typical response time (τ_{res}) and recovery time (τ_{recov}) of Pd-loaded SnO_2 to 20 ppm toluene are about 0.48 s and 5.5 s, respectively. Compared with toluene sensing performances of other SnO_2-based sensors, as summarized in Table 1 [14,29–33], our Pd-loaded SnO_2 hollow spheres show remarkably enhanced response and shortened response time at relatively low toluene concentration. The improved sensing performances of our Pd-loaded SnO_2 can be attributed to the ultrathin nanorod-assembled hollow structure and the effect of loaded Pd particles.

3.3. Gas sensing mechanism

As one of the most typical n-type semiconducting oxides for gas detection, the widely accepted sensing mechanism for SnO_2 nanostructures can be understood via space-charge model [34], which involves two reverse charge transfer behaviors when SnO_2 is exposed to air and testing gas ambiences, respectively. When SnO_2-based sensor is exposed to air ambience, oxygen molecules can firstly be physically adsorbed on the surface of SnO_2 sample and subsequently trap the free electrons (carriers) from the conduction band of SnO_2 sample due to its stronger electron affinity to form chemisorbed oxygen species (O_2^-, O^-, or O^{2-}). After the continuous chemisorption of oxygen molecules to reach certain equilibrium, the unceasing outward flow of free electrons eventually leads to the formation of thick electron depletion layer on SnO_2 surface and stable high resistance, as schematically illustrated in Fig. 10a. When the SnO_2 sensor is exposed to the reducing gas of toluene, these chemisorbed oxygen species can take part in the desorption reaction with toluene molecules and release the trapped electrons back into the conduction band of SnO_2 sample. Conversely, the returned free electrons eventually result in a decrease of the thickness of the surface depletion layer and stable low resistance through continuous desorption of the surface oxygen species to reach another equilibrium, as illustrated in Fig. 10b. Based on this understanding, the variation of characteristic resistance can be discerned to establish the one-to-one correspondence between the sensing behaviors and characteristics.

Based on the basic sensing principle and the design strategies of high-performance gas sensing materials proposed by Yamazoe et al. [2,35], the enhanced toluene sensing performances of our Pd-loaded SnO_2 products are most likely to be ascribed to the following several aspects: (i) The first aspect can be attributed to the reasonable configuration of SnO_2 hollow spheres. The BET result and the corresponding pore-size distribution (Fig. 4b) explicitly verify that the as-obtained SnO_2 spheres show hollow interiors and well-aligned porous structures without scarifying high surface area [36]. The nanorod-assembled porous SnO_2 hollow spheres provide numerous well-aligned channels for the unhampered diffusion of gas molecules to reach or leave the sensing surface. Simultaneously, this less-agglomerated configuration guarantees a high contact area for the efficient absorption and subsequent interaction between oxygen species and target gas. (ii) Relative to the traditional point-to-point contact of neighboring nanoparticle-assembled spheres, the multipoint contact form of our spheres means a broader conductive channel of electrons transfer between neighboring spheres (Fig. 10c), meaning an improving probability for the decreased thickness and height of the contacting potential barrier. The multipoint contact form also has a positive impact on the improvement of gas sensing performances [14]. (iii) According to the space charge model [37], L_d (Debye length) can be expressed by:

$$L_d = \left(\frac{\varepsilon k_B T}{q^2 n_c}\right)^{1/2} \quad (3)$$

where ε is the static dielectric constant, k_B is the Boltzmann's constant, T is the absolute temperature, n_c is the carrier concentration, and q is the electrical charge of the carrier. These parameters, which are used to represent typical values for SnO_2-based sensors, are $\varepsilon = 9.0 \times 8.85 \times 10^{-12}$ F m^{-1}, $k_B = 1.38 \times 10^{-23}$ J K^{-1}, $T = 523$ K (optimal temperature), and $q = 1.6 \times 10^{-19}$C. The electron density of SnO_2 is normally about 10^{15}–10^{18} cm^{-3}. According to Eq. (3) with the introduction of $n_c = 5.1 \times 10^{17}$ cm^{-3}, the calculated L_d is about

Table 1
Comparison between Pd-loaded SnO_2 hollow spheres in the present work and other SnO_2-based nanostructures.

Materials	Temperature (°C)	Response	Detection limit (ppm)	Response recovery times (s)		Reference
Pd-loaded SnO_2 hollow spheres	230	52.9 (20 ppm)	0.1	0.48	5.5	This work
double-shelled SnO_2 cages	250	33.4 (20 ppm)	1	2.3	5.8	[14]
SnO_2-ZnO hollow nanofibers	190	15.6 (50 ppm)	1	6–11	12–23	[29]
Pd-loaded flowerlike SnO_2	250	17.4 (10 ppm)	0.08	~10	>400	[30]
NiO-SnO_2 nanofibers	330	11 (50 ppm)	50	11.2	4	[31]
meso-macroporous SnO_2	220	3 (100 ppm)	10	5	38	[32]
SnO_2@SnO_2 cuboctahedra	250	28.6 (20 ppm)	1	1.8	4.1	[33]

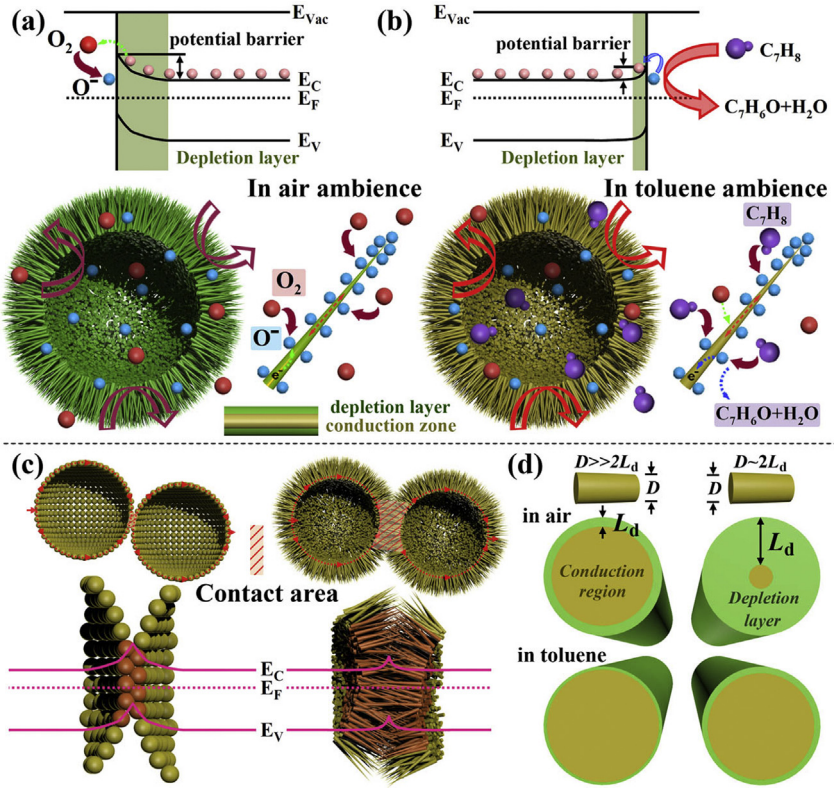

Fig. 10. Schematic views of possible sensing mechanism and surface processes of nanorod-assembled SnO_2 hollow spheres associated with sensing reaction with (a) ambient oxygen and (b) testing toluene, (c) energy band representation of the interface region associated with the point-to-point (left) and multipoint contacts (right), and (d) schematic view of depletion layer on the cross section from nanorods with different diameters.

6.6 nm. Thus, because the nanorod diameter of nanorod subunits is so thin that reaches a scale comparable with the Debye length (electron depletion layer thickness, $D \sim 2L_d$), the complete depletion of electrons will be achieved, and the amount of oxygen that can be adsorbed and ionized is maximized (Fig. 10d). From these points of view, the reasonable porous and hollow structure makes pure SnO_2 more efficient to participate in gas detection.

(iv) The toluene-sensing performances of pure SnO_2 spheres can further be promoted by the additional effects of Pd/PdO [2,38]. The first aspect is based on catalytic activity of PdO due to the improved capability of oxygen dissociation. The surface Pd atoms are easily bonded with oxygen molecules to form PdO in air ambience, and the resulting complexes are readily dissociated and release oxygen atoms at a relatively low temperature. Compared with unloaded SnO_2, PdO can catalytically activate the dissociation process of oxygen molecules and increase the quantity of adsorbed oxygen ions, resulting in faster and greater degree of electron depletion at the interface regions than that of unloaded SnO_2 and eventually enhancing sensing reaction and performances. Another aspect is related to the spillover effect, which plays an important role in the interface interactions [2]. The surface PdO can change its oxidation state to facilitate the generation of surface Pd phase in the reducing toluene ambient and be reoxidized in air ambiance [39]. The vacant sites for adsorption on PdO/Pd will physically adsorb oxygen/toluene molecules onto the surfaces and simultaneously spillover onto the surface of SnO_2, activating the sensing reaction between toluene molecules and oxygen species and eventually improving the response. In this work, besides the hollow and porous structural merits, the additional effects of loaded Pd/PdO on the whole sensing process further improve the sensing performances for gas detection.

4. Conclusions

In summary, Pd-doped SnO_2 hollow spheres have been successfully prepared via a facile one-pot hydrothermal process and subsequent Pd-loaded treatment. The pure and Pd-loaded SnO_2 hollow spheres exhibit interior cavities and porous shells, which are hierarchically constructed of numerous rodlike SnO_2 primary building blocks with the ultrathin diameter of about 5–10 nm. The synthetic time-dependent morphology and structure evolution confirm that the formation of nanorod-assembled SnO_2 hollow spheres is addressed in terms of the Ostwald ripening in the hydrothermal process. The gas-sensing results confirm that the

doping Pd particles can significantly enhance the toluene sensing performances due to the less-agglomerated hollow structure with ultrathin rodlike subunits and the effect of loaded Pd particles. This phenomenon exhibits the potential research value to further adjust the gas-sensing performances and understand the basic sensing reaction scheme of catalytic sensitization.

Acknowledgements

This research work was financially supported by the Natural Science Foundation of China (Grant nos. 51372095, 51402122, and 61376122), the Research Fund for the Doctoral Program of Higher Education of China (no. 20120061120039), Independent Project of State Key Laboratory of Applied Optics, Changchun Institute of Optics, Fine Mechanics and Physics, Chinese Academy of Sciences (CAS), and Youth Innovation Promotion Association of CAS (no. 2014193).

Appendix A. Supplementary data

Supplementary data associated with this article can be found, in the online version, at http://dx.doi.org/10.1016/j.snb.2016.11.153.

References

[1] T. Seiyama, A. Kato, K. Fujushi, M. Nagatani, Study on a detector for gaseous components using semiconductive thin films, Anatlyt. Chem. 38 (1962) 1069–1073.
[2] N. Yamazoe, New approaches for improving semiconductor gas sensors, Sens. Actuators B 5 (1991) 7–19.
[3] J. Hu, M. Chen, X.S. Fang, L.M. Wu, Fabrication and application of inorganic hollow spheres, Chem. Soc. Rev. 40 (2011) 5472–5491.
[4] X.W. Lou, L.A. Archer, Z.C. Yang, Hollow micro-/nanostructures: synthesis and applications, Adv. Mater. 20 (2008) 3987–4019.
[5] Y. Yin, R. Rioux, C.K. Erdonmcz, S. Hushes, G.A. Somorjai, A.P. Alivisatos, Formation of hollow nanocrystals through the nanoscale Kirkendall effect, Science 304 (2004) 711–714.
[6] Y.G. Sun, B.T. Mayers, Y.N. Xia, Template-engaged replacement reaction: a one-step approach to the large-scale synthesis of metal nanostructures with hollow interiors, Nano Lett. 2 (2002) 481–485.
[7] Y.G. Sun, Y.N. Xia, Shape-controlled synthesis of gold and silver nanoparticles, Science 298 (2002) 2176–2179.
[8] G.J. Li, X.H. Zhang, S. Kawi, Relationships between sensitivity catalytic activity, and surface areas of SnO_2 gas sensors, Sens. Actuators B 60 (1999) 64–70.
[9] L.P. Qin, J.Q. Xu, X.W. Dong, Q.Y. Pan, Z.X. Cheng, Q. Xiang, F. Li, The template-free synthesis of square-shaped SnO_2 nanowires: the temperature effect and acetone gas sensors, Nanotechnology 19 (2008) 185705.
[10] Y. Shimizu, T. Hyodo, M. Egashira, Mesoporous semiconducting oxides for gas sensor application, J. Eur. Ceram. Soc. 24 (2004) 1389–1398.
[11] Y.L. Wang, X.C. Jiang, Y.N. Xia, A solution-phase, precursor route to poly-crystalline SnO_2 nanowires that can be used for gas sensing under ambient conditions, J. Am. Chem. Soc. 125 (2003) 16171–16176.
[12] Y.E. Chang, D.Y. Youn, G. Ankonina, D.J. Yang, H.G. Kim, A. Rothschild, I.D. Kim, Fabrication and gas sensing properties of hollow SnO_2 hemispheres, Chem. Commun. 45 (2009) 4019–4021.
[13] L.L. Wang, Z. Lou, T. Zhang, H.T. Fan, X.J. Xu, Facile synthesis of hierarchical SnO_2 semiconductor microspheres for gas sensor application, Sens. Actuators B 155 (2011) 285–289.
[14] Y.F. Bing, Y. Zeng, C. Liu, L. Qiao, W.T. Zheng, Synthesis of double-shelled SnO_2 nano-polyhedra and their improved gas sensing properties, Nanoscale 7 (2015) 3276–3284.
[15] N.S. Ramgir, I.S. Mulla, K.P. Vijayamohanan, A room temperature nitric oxide sensor actualized from Ru-doped SnO_2 nanowires, Sens. Actuators B 107 (2005) 708–715.
[16] A. Kolmakov, D.O. Klenov, Y. Lilach, S. Stemmer, M. Moskovits, Enhanced gas sensing by individual SnO_2 nanowires and nanobelts functionalized with Pd catalyst particles, Nano Lett. 5 (2005) 667–673.
[17] Y.C. Lee, H. Huang, O.K. Tan, M.S. Tse, Semiconductor gas sensor based on Pd-doped SnO_2 nanorod thin films, Sen. Actuators B 132 (2008) 239–242.
[18] G. Korotcenkov, V. Brinzari, Y. Boris, M. Ivanov, J. Schwank, J. Morante, Influence of surface Pd doping on gas sensing characteristics of SnO_2 thin films deposited by spray pirolysis, Thin Solid Films 436 (2003) 119–126.
[19] M.V. Vaishampayan, R.G. Deshmukh, I.S. Mulla, Influence of Pd doping on morphology and LPG response of SnO_2, Sens. Actuators B 131 (2008) 665–672.
[20] Y. Zeng, T. Zhang, L.J. Wang, M.H. Kang, H.T. Fan, R. Wang, Y. He, Enhanced toluene sensing characteristics of TiO_2-doped flowerlike ZnO nanostructures, Sens. Actuators B 140 (2009) 73–78.
[21] Y. Zeng, L. Qiao, Y.F. Bing, M. Wen, B. Zou, W.T. Zheng, T. Zhang, G.T. Zou, Development of microstructure CO sensor based on hierarchically porous ZnO nanosheet thin films, Sens. Actuators B 173 (2012) 897–902.
[22] Y.G. Zheng, J. Wang, P.J. Yao, Formaldehyde sensing properties of electrospun NiO-doped SnO_2 nanofibers, Sens. Actuators B 156 (2011) 723–730.
[23] D. Andreeva, T. Tabakova, V. Idakiev, P. Christov, R. Giovanoli, Au/α-Fe_2O_3 catalyst for water-gas shift reaction prepared by deposition-precipitation, Appl. Catal. A 169 (1998) 9–14.
[24] H. Zhang, Z. Li, L. Liu, X. Xu, Z. Wang, W. Wang, W. Zheng, B. Dong, C. Wang, Enhancement of hydrogen monitoring properties based on Pd-SnO_2 composite nanofibers, Sens. Actuators B 147 (2010) 111–115.
[25] D.F. Zhang, L.D. Sun, J.L. Yin, C.H. Yan, Low-temperature fabrication of highly crystalline SnO_2 nanorods, Adv. Mater. 15 (2003) 1022–1025.
[26] Y.G. Li, L. Qiao, L.L. Wang, Y. Zeng, W.Y. Fu, H.B. Yang, Synthesis of self-assembled 3D hollow microspheres of SnO_2 with an enhanced gas sensing performance, Appl. Surf. Sci. 285 (2013) 130–135.
[27] Z. Zhang, H. Sun, X. Shao, D. Li, H. Yu, M. Han, Three-dimensionally oriented aggregation of a few hundred nanoparticles into monocrystalline architectures, Adv. Mater. 17 (2005) 42–47.
[28] W.J. Li, E.W. Shi, W.Z. Zhong, Z.W. Yin, Growth mechanism and growth habit of oxide crystals, J. Cryst. Growth 203 (1999) 186–196.
[29] S.H. Wei, Y. Zhang, M.H. Zhou, Toluene sensing properties of SnO_2–ZnO hollow nanofibers fabricated from single capillary electrospinning, Solid State Commun. 151 (2011) 895–899.
[30] J.L. Tian, J. Wang, Y.W. Hao, H.Y. Du, X.G. Li, Toluene sensing properties of porous Pd-loaded flower-like SnO_2 microspheres, Sens. Actuators B 202 (2014) 795–802.
[31] L. Liu, Y. Zhang, G.G. Wang, S.C. Li, L.Y. Wang, Y. Han, X.X. Jiang, A.G. Wei, High toluene sensing properties of NiO-SnO_2 composite nanofiber sensors operating at 330 °C, Sens. Actuators B 160 (2011) 448–454.
[32] H.H. Li, F.L. Meng, J.Y. Liu, Y.F. Sun, Z. Jin, L.T. Kong, Y.J. Hu, J.H. Liu, Synthesis and gas sensing properties of hierarchical meso-macroporous SnO_2 for detection of indoor air pollutants, Sens. Actuators B 166–167 (2012) 519–525.
[33] Y.F. Bing, C. Liu, L. Qiao, Y. Zeng, S.S. Yu, Z.Z. Liang, J.P. Liu, J.Z. Luo, W.T. Zheng, Multistep synthesis of non-spherical SnO_2@SnO_2 yolk-shell cuboctahedra with nanoparticle-assembled porous structure for toluene detection, Sens. Actuators B 231 (2016) 365–375.
[34] M. Egashira, Y. Shimizu, Y. Takao, S. Sako, Variations in I–V characteristics of oxide semiconductors induced by oxidizing gases, Sens. Actuators B 35 (1996) 62–67.
[35] N. Yamazoe, G. Sakai, K. Shimanoe, Oxide semiconductor gas sensors, Catal. Surv. Asia 7 (2003) 63–75.
[36] J.H. Lee, Gas sensors using hierarchical and hollow oxide nanostructures: overview, Sens. Actuators B 140 (2009) 319–336.
[37] N. Hongsith, E. Wongrat, T. Kerdcharoen, S. Choopun, Sensor response formula for sensor based on ZnO nanostructures, Sens. Actuators B 144 (2010) 67–72.
[38] S.W. Choi, S.S. Kim, Room temperature CO sensing of selectively grown networked ZnO nanowires by Pd nanodot functionalization, Sens. Actuators B 168 (2012) 8–13.
[39] Y. Shen, T. Yamazaki, Z. Liu, D. Meng, T. Kikuta, N. Nakatkani, M. Satio, M. Mori, Microstructure and H_2 gas sensing properties of undoped and Pd-doped SnO_2 nanowires, Sens. Actuators B 135 (2009) 524–529.

Biographies

Kan Zhang received his PhD degree from College of Materials Science and Engineering, Jilin University, China in 2014 majored in Materials Physics and Chemistry. He was appointed the lecture in Department of materials science, Jilin University in July, 2015. Now, he focuses on preparation and characterization the low dimension nanomaterials.

Xin Yang is working for his MS degree from the Department of Materials Science, majoring in Materials Physics and Chemistry, Jilin University. He is interested in the design and preparation of semiconducting oxides with hierarchical and porous nanostructures.

Yanzhe Wang is working for his PhD degree, majoring in Materials Physics and Chemistry, in Jilin University. He is interested in the synthesis and applications of semiconducting oxides with hollow and porous structures.

Yifei Bing received his BE degree from the Department of Materials Science, Jilin University, China in 2010. Now he is working for his PhD degree, majoring in Materials Physics and Chemistry, in Jilin University. He is interested in the synthesis and applications of graphene composites, functional nanomaterials, and gas sensors.

Liang Qiao is an associate professor at the College of Science, Changchun University, China. She received her PhD degree from the Department of Materials Science, Jilin University, China in 2007. Now, she is engaged in the simulation of the gas sensing properties of semiconducting functional materials, and graphene nanocomposites.

Zhongzhu Liang is a professor in State Key Laboratory of Applied Optics, Changchun Institute of Optics, Fine Mechanics and Physics, Chinese Academy of Sciences. He received his PhD degree from State Key Laboratory of Superhard Materials, Jilin University, China in 2007. Now, he is engaged in micro optical electro-mechanical-system, plasmonics and sensors.

Shansheng Yu is an associate professor at the Department of Materials Science, Jilin University, China. He received his PhD degree from the Department of Materials Science, Jilin University, China in 2007. Now, he is engaged in the simulation of the gas sensing properties of semiconducting functional materials, and graphene nanocomposites.

Yi Zeng received his MS degree from State Key Laboratory of Superhard Materials, Jilin University, China in 2007. He received his PhD degree from College of Electronic Science and Engineering, Jilin University, China in 2010 majored in Microelectronics and Solid state Electronics. He was appointed the associate professor in Department of Materials Science, Jilin University in October, 2012. Now, he is engaged in the synthesis and characterization of the semiconducting functional materials, nanocomposites, and gas sensors.

Weitao Zheng is Professor and Dean at the School of Materials Science and Engineering, Jilin University, China. He obtained his PhD degree from Jilin University in the field of condensed matter physics in 1990. His research interests concentrate on superhard thin film materials and carbon related nanomaterials and he has published more than 200 papers in peer-refereeing international journals.